

Energy Distribution Characteristics of Magnetically Coupled Resonant Wireless Power Transfer Systems Considering Four Basic Reactive Power Compensations

Wanlu Li*, Quandi Wang, Jianwei Kang, and Yingcong Wang

Abstract—To realize the attractive Wifi-type magnetically coupled resonant (MCR) wireless power transfer (WPT) techniques, not only the optimization of power and efficiency but also the spatial energy distribution characteristics (EDCs) should be considered. In this paper, the EDCs of three two-coil systems including an alignment system and systems with an angular and lateral misalignment are explored by the Poynting vector, and unified expressions of the active power density (APD) and reactive power density (RPD) are provided. Also, it is found that the APD is mainly distributed in the transmission path, and the RPD is mainly composed of three parts. When the phase difference between the currents in the transmitter and receiver tends to be $\pi/2$, the APD increases, and RPD decreases. The active power through an arbitrary infinite plane which intersects the transmission path but does not intersect the coupler is found equal to the transferred active power of the system, which is consistent with the results obtained by the circuit theory. Furthermore, the directionality of the APD is determined, and the APD is utilized to explain the coupling impedance in circuit theory. Then four basic reactive power compensations are considered, and it is recommended to use heavy load for the system with parallel compensation on the secondary side. Finally, the theoretical analysis is verified by simulation and experiment. This paper provides a significant reference for the analysis and design of the MCR WPT system and the improvement of the electromagnetic environment around the system.

1. INTRODUCTION

Magnetically coupled resonant (MCR) wireless power transfer (WPT) utilizes the magnetic coupling of the system coils and impedance matching by means of circuit resonance, and thus can achieve considerable power transmission over a long distance. Due to the advantages of convenient charging, aesthetics, safe operation, and dramatically solving limited battery storage problems, the techniques have been utilized in many technical applications, such as electric vehicles (EVs) [1–3], consumer electronics [4–6], implantable biomedical devices [7, 8], unmanned aerial vehicles (UAVs) [9, 10], and sensors [11, 12]. However, the techniques also face many challenges including Wi-Fi-power technique or WPT with spatial freedom [13]. Not only does the challenge involve how to maintain constant output power for the system when receiver offsets, or orientation changes, but the high energy density around the system would not threaten the electromagnetic safety of people around the system. At present, most of the analysis and optimization of the systems focus on the power or efficiency, and are mainly based on the circuit theory [14–18], which is difficult to analyze electromagnetic environment and energy flow in space. Accordingly, the energy distribution characteristics (EDCs) of the MCR WPT systems attract attentions from researchers [19–21]. For instance, Faria explored the EDCs of a system that only contained a transmitting coil by means of Poynting vector [19]. Liu et al. analyzed the Poynting vector

Received 16 July 2019, Accepted 23 September 2019, Scheduled 7 October 2019

* Corresponding author: Wanlu Li (1397228682@qq.com).

The authors are with the State Key Laboratory of Power Transmission Equipment & System Security and New Technology, Chongqing University, Chongqing, China.

distribution of a two-coil MCR WPT system considering different loading points and load values [20], but no quantitative studies have been conducted. Guo et al. analyzed the transmission characteristics of a system with different loads and concluded that when the load was inductive or capacitive, the real part of the Poynting vector was zero, and the system could not transmit power, whereas when the load was resistive, the power could be transmitted [21]. However, the Poynting vector formula in [21] was derived based on the magnetic dipole, which is suitable for the calculation of the electromagnetic field (EMF) in the far field and for high frequencies. Its applicability for analyzing the near-field EDCs of the WPT system generally below 13.56 MHz may be problematic. Previous studies have only focused on alignment systems, not considering systems with an angular or lateral misalignment, and also not considering different reactive power compensations. All in all, research on the EDCs of the system is still far from enough.

In this paper, we explore the EDCs of three two-coil MCR WPT systems including an alignment system and systems with a lateral and angular misalignment (see Figure 1) based on Biot-Savart's law and Poynting vector theory. For these three systems, unified expressions of active power density (APD) and reactive power density (RPD) are provided. It is found that the APD is mainly distributed in the transmission path, while the RPD is mainly composed of three parts, two of which are separately generated by transmitter (Tx) and transmitter (Rx) and distributed in the vicinity. The third part is an interactive RPD, which is mainly distributed in the transmission path. Then the quantitative analysis of the APD reveals that the active power through an arbitrary infinite plane which intersects the transmission path but does not intersect the coupler (a combination of the Tx and Rx) is equal to the transferred active power of the system, which is consistent with the results derived from the circuit theory. Then based on the EDCs of the system, four basic reactive power compensations for MCR WPT systems, i.e., (a) primary series-second series (SS), (b) primary parallel-second series (PS), (c) primary series-second parallel (SP), (d) primary parallel-second parallel (PP), are considered. Finally, the correctness of the theoretical results are verified by simulation and experiment.

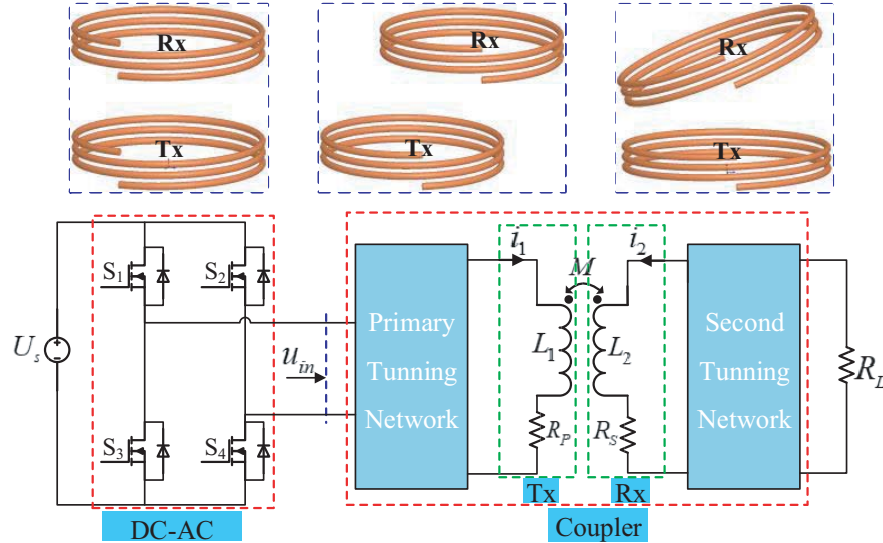


Figure 1. Three MCR WPT systems including an alignment system, systems with a lateral and angular misalignment and their equivalent circuit model considering four basic reactive power compensations, i.e., SS, PS, SP and PP.

The paper is organized as follows. The EDCs of three two-coil systems are analyzed based on the Poynting vector in Section 2. Then the quantitative research on the APD is presented in Section 3, and four basic reactive power compensations are considered. In Section 4, the frequency-domain method and simulation are utilized to verify the correctness of the theoretical calculation, and experiment is conducted to verify that heavy load helps improve the power transfer efficiency (PTE) of the system with parallel compensation on the secondary side. Section 5 provides a summary of the paper.

2. ENERGY DISTRIBUTION CHARACTERISTICS OF THREE TWO-COIL MCR SYSTEMS

First the expressions of the EDCs considering an arbitrary MCR WPT system, i.e., an alignment system, or a system with a lateral or angular misalignment, are to be derived. Since the alignment system can be regarded as a special case of the latter two systems, below we will discuss the energy flow in two cases, one case is that the Rx has a horizontal misalignment, and the other is that the Rx has an angular rotation.

2.1. EDCs of MCR WPT System Where Rx Has a Horizontal Misalignment

Based on the Biot-Savar's law, the magnetic vector potential \mathbf{A} at arbitrary point $p(x, y, z)$ (Figure 2) around a single filamentary loop is obtained.

$$\mathbf{A} = \frac{\mu i}{4\pi} \oint_{\Gamma} \frac{d\mathbf{l}'}{r} \quad (1)$$

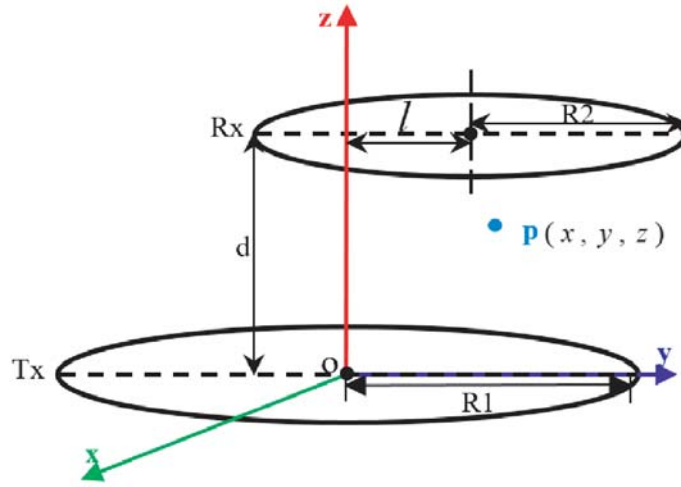


Figure 2. MCR WPT system with an Rx horizontal offset distance of l .

Then the electric field strength and magnetic field strength are obtained respectively based on Maxwell's equations.

$$\mathbf{E} = -\nabla\varphi - \frac{\partial\mathbf{A}}{\partial t}, \quad \mathbf{H} = \frac{1}{\mu}\nabla \times \mathbf{A}. \quad (2)$$

When only non-source areas are considered, Eq. (2) can be simplified as

$$\mathbf{E} = -\frac{\partial\mathbf{A}}{\partial t}, \quad \mathbf{H} = \frac{1}{\mu}\nabla \times \mathbf{A}. \quad (3)$$

According to the superposition principle, the electromagnetic field values at point p are obtained,

$$\begin{aligned} \mathbf{E} &= \mathbf{E}_1 + \mathbf{E}_2 = -\frac{\partial}{\partial t} [(P_{x1}i_1 + P_{x2}i_2) \cdot \mathbf{e}_x + (P_{y1}i_1 + P_{y2}i_2) \cdot \mathbf{e}_y], \\ \mathbf{H} &= \mathbf{H}_1 + \mathbf{H}_2 = (T_{x1}i_1 + T_{x2}i_2) \cdot \mathbf{e}_x + (T_{y1}i_1 + T_{y2}i_2) \cdot \mathbf{e}_y + (T_{z1}i_1 + T_{z2}i_2) \cdot \mathbf{e}_z. \end{aligned} \quad (4)$$

where

$$\begin{cases} P_{xi} = \frac{\mu_0 R_i}{4\pi} \int_0^{2\pi} \frac{-\sin\theta}{\sqrt{(x - R_i \cos\theta)^2 + [y - (i-1) \cdot l - R_i \sin\theta]^2 + [z - (i-1) \cdot d]^2}} d\theta, \\ P_{yi} = \frac{\mu_0 R_i}{4\pi} \int_0^{2\pi} \frac{\cos\theta}{\sqrt{(x - R_i \cos\theta)^2 + [y - (i-1) \cdot l - R_i \sin\theta]^2 + [z - (i-1) \cdot d]^2}} d\theta. \end{cases}$$

$$\begin{cases} T_{xi} = \frac{R_i}{4\pi} \int_0^{2\pi} \frac{[z - (i-1) \cdot d] \cdot \cos \theta}{\{(x - R_i \cos \theta)^2 + [y - (i-1) \cdot l - R_i \sin \theta]^2 + [z - (i-1) \cdot d]^2\}^{3/2}} d\theta, \\ T_{yi} = \frac{R_i}{4\pi} \int_0^{2\pi} \frac{[z - (i-1) \cdot d] \cdot \sin \theta}{\{(x - R_i \cos \theta)^2 + [y - (i-1) \cdot l - R_i \sin \theta]^2 + [z - (i-1) \cdot d]^2\}^{3/2}} d\theta, \\ T_{zi} = \frac{R_i}{4\pi} \int_0^{2\pi} \frac{R_i - \{x \cos \theta + [y - (i-1) \cdot l] \cdot \sin \theta\}}{\{(x - R_i \cos \theta)^2 + [y - (i-1) \cdot l - R_i \sin \theta]^2 + [z - (i-1) \cdot d]^2\}^{3/2}} d\theta. \end{cases} \quad (i = 1, 2).$$

P , T are the parameters that characterize the geometrical and material properties; $i = 1, 2$ respectively represent the values corresponding to Tx and Rx; R_1 (R_2) represents the radius of Tx (Rx); l indicates the offset distance; d indicates the transmission distance; μ_0 indicates the magnetic permeability of air.

Then the power passing through a unit area perpendicular to the energy flow direction at a point p around MCR WPT system based on Poynting vector theory in [22] can be obtained as follows,

$$\begin{aligned} \mathbf{S} = \mathbf{E} \times \mathbf{H} = & \frac{\partial i_1}{\partial t} i_1 \cdot [-P_{y1} T_{z1} \cdot \mathbf{e}_x + P_{x1} T_{z1} \cdot \mathbf{e}_y + (-P_{x1} T_{y1} + P_{y1} T_{x1}) \cdot \mathbf{e}_z] \\ & + \frac{\partial i_2}{\partial t} i_2 \cdot [-P_{y2} T_{z2} \cdot \mathbf{e}_x + P_{x2} T_{z2} \cdot \mathbf{e}_y + (-P_{x2} T_{y2} + P_{y2} T_{x2}) \cdot \mathbf{e}_z] \\ & + \frac{\partial i_1}{\partial t} i_2 \cdot [-P_{y1} T_{z2} \cdot \mathbf{e}_x + P_{x1} T_{z2} \cdot \mathbf{e}_y + (-P_{x1} T_{y2} + P_{y1} T_{x2}) \cdot \mathbf{e}_z] \\ & + \frac{\partial i_2}{\partial t} i_1 \cdot [-P_{y2} T_{z1} \cdot \mathbf{e}_x + P_{x2} T_{z1} \cdot \mathbf{e}_y + (-P_{x2} T_{y1} + P_{y2} T_{x1}) \cdot \mathbf{e}_z] \end{aligned} \quad (5)$$

where i_1 , i_2 are the currents in Tx and Rx, respectively, which can be expressed as

$$i_1 = \sqrt{2} I_1 \cos(\omega t), \quad i_2 = \sqrt{2} I_2 \cos(\omega t - \alpha).$$

where I_1 (I_2) represents the root mean square (RMS) value of i_1 (i_2), respectively; α is the lagging phase of the current in the Rx behind the current in the Tx.

Then Eq. (5) can be rewritten as

$$\mathbf{S} = \mathbf{S}_{p11} + \mathbf{S}_{p22} + \mathbf{S}_{p12} + \mathbf{S}_{p21} \quad (6)$$

where

$$\begin{aligned} \mathbf{S}_{p11} &= -\omega I_1^2 \sin(2\omega t) \cdot [-P_{y1} T_{z1} \cdot \mathbf{e}_x + P_{x1} T_{z1} \cdot \mathbf{e}_y + (-P_{x1} T_{y1} + P_{y1} T_{x1}) \cdot \mathbf{e}_z], \\ \mathbf{S}_{p22} &= -\omega I_2^2 \sin(2\omega t - 2\alpha) \cdot [-P_{y2} T_{z2} \cdot \mathbf{e}_x + P_{x2} T_{z2} \cdot \mathbf{e}_y + (-P_{x2} T_{y2} + P_{y2} T_{x2}) \cdot \mathbf{e}_z], \\ \mathbf{S}_{p12} &= -\omega I_1 I_2 \cdot \{\cos \alpha \cdot \sin(2\omega t) + \sin \alpha \cdot [1 - \cos(2\omega t)]\} \\ &\quad \cdot [-P_{y1} T_{z2} \cdot \mathbf{e}_x + P_{x1} T_{z2} \cdot \mathbf{e}_y + (-P_{x1} T_{y2} + P_{y1} T_{x2}) \cdot \mathbf{e}_z], \\ \mathbf{S}_{p21} &= -\omega I_1 I_2 \cdot \{\cos \alpha \cdot \sin(2\omega t) - \sin \alpha \cdot [1 + \cos(2\omega t)]\} \\ &\quad \cdot [-P_{y2} T_{z1} \cdot \mathbf{e}_x + P_{x2} T_{z1} \cdot \mathbf{e}_y + (-P_{x2} T_{y1} + P_{y2} T_{x1}) \cdot \mathbf{e}_z]. \end{aligned} \quad (7)$$

Formulas (6) and (7) are the transient expression of the Poynting vector of the MCR WPT system. S_{p12} and S_{p21} contain $\sin \alpha \cdot [1 - \cos(2\omega t)]$ and $\sin \alpha \cdot [1 + \cos(2\omega t)]$, respectively, and both oscillate around 1 and are always non-negative. In a cycle $T = 2\pi/\omega$, the time average value is active power density (APD), which is recorded as \mathbf{S}_{av} and can be expressed as

$$\begin{aligned} \mathbf{S}_{av} &= \frac{1}{T} \int_0^T S(x, y, z, t) dt \\ &= \omega I_1 I_2 \sin \alpha \cdot [(P_{y1} T_{z2} - P_{y2} T_{z1}) \cdot \mathbf{e}_x \\ &\quad + (P_{x2} T_{z1} - P_{x1} T_{z2}) \cdot \mathbf{e}_y + (P_{x1} T_{y2} - P_{x2} T_{y1} + P_{y2} T_{x1} - P_{y1} T_{x2}) \cdot \mathbf{e}_z] \end{aligned} \quad (8)$$

which indicates that APD is proportional to angular frequency, the RMS values of the currents in the Tx and Rx, and $\sin \alpha$. S_{p11} and S_{p22} contain $\sin(2\omega t)$, and S_{p12} and S_{p21} contain $\cos \alpha \cdot \sin(2\omega t)$. They all oscillate around 0, which means that the power is generated at one moment and dissipated at the other, while the mean value is zero. Considering that the direction of the reactive power density (RPD) of the coils is outward, the RPD generated by Tx (or Rx) can be expressed as follows [22],

$$\mathbf{S}_{im-i} = \omega I_i^2 \cdot [-P_{yi} T_{zi} \cdot \mathbf{e}_x + P_{xi} T_{zi} \cdot \mathbf{e}_y + (-P_{xi} T_{yi} + P_{yi} T_{xi}) \cdot \mathbf{e}_z] \quad (i = 1, 2) \quad (9)$$

which reveals that the RPD generated by Tx (Rx) is proportional to the square of the RMS values of the currents in the Tx (Rx) as well as angular frequency. The interactive RPD between the Tx and Rx is

$$\begin{aligned} \mathbf{S}_{im_{12}} = \omega I_1 I_2 \cdot \cos \alpha \cdot [(P_{y1} T_{z2} + P_{y2} T_{z1}) \cdot \mathbf{e}_x - (P_{x1} T_{z2} + P_{x2} T_{z1}) \cdot \mathbf{e}_y \\ + (P_{x1} T_{y2} + P_{x2} T_{y1} - P_{y1} T_{x2} - P_{y2} T_{x1}) \cdot \mathbf{e}_z] \end{aligned} \quad (10)$$

which means that the interactive RPD is proportional to $\cos \alpha$.

Furthermore, since P and T respectively approximately satisfy $\frac{1}{r}$ and $\frac{1}{r^2}$ attenuation with distance r from the field point to the coils, APD and RPD approximately satisfy $\frac{1}{r^3}$ attenuation with r , thus $S_{im_{12}}$ near the Tx (or the $S_{im_{21}}$ near the Rx) could be much larger than those in other areas, whereas S_{av} and $S_{im_{12}}$ could have large values in the transmission path between the two coils. So the APD of the MCR WPT system is mainly distributed in the transmission path, whereas the RPD is mainly composed of three parts, two of which are near the Tx and Rx, respectively, and the third part is distributed in the transmission path. The existence of the third part $S_{im_{12}}$ mainly depends on the phase difference between the two currents in the Tx and Rx. When the phase difference is $\pi/2$, this part of the RPD no longer exists.

2.2. EDCs of MCR WPT System Where Rx Has an Angular Rotation

Similarly, the expressions of the electromagnetic field and APD and RPD can be obtained when Rx has an angular rotation (Figure 3). The forms of the expressions are same as the previous ones, except that parameters P and T corresponding to Rx are changed. P and T parameters corresponding to Rx are respectively as follows at this time.

$$\left\{ \begin{aligned} P_{x2} &= \frac{\mu_0 R_2}{4\pi} \int_0^{2\pi} \frac{-\sin \theta}{\sqrt{(x - R_2 \cos \theta)^2 + (y - R_2 \sin \theta \cos \beta)^2 + (z - R_2 \sin \theta \sin \beta - d)^2}} d\theta, \\ P_{y2} &= \frac{\mu_0 R_2}{4\pi} \int_0^{2\pi} \frac{\cos \beta \cos \theta}{\sqrt{(x - R_2 \cos \theta)^2 + (y - R_2 \sin \theta \cos \beta)^2 + (z - R_2 \sin \theta \sin \beta - d)^2}} d\theta, \\ P_{z2} &= \frac{\mu_0 R_2}{4\pi} \int_0^{2\pi} \frac{\sin \beta \cos \theta}{\sqrt{(x - R_2 \cos \theta)^2 + (y - R_2 \sin \theta \cos \beta)^2 + (z - R_2 \sin \theta \sin \beta - d)^2}} d\theta. \end{aligned} \right. \quad (11)$$

$$\left\{ \begin{aligned} T_{x2} &= \frac{R_2}{4\pi} \int_0^{2\pi} \frac{-y \sin \beta \cos \theta + (z - d) \cos \beta \cos \theta}{[(x - R_2 \cos \theta)^2 + (y - R_2 \sin \theta \cos \beta)^2 + (z - R_2 \sin \theta \sin \beta - d)^2]^{3/2}} d\theta, \\ T_{y2} &= \frac{R_2}{4\pi} \int_0^{2\pi} \frac{-R_2 \sin \beta + (z - d) \sin \theta + x \sin \beta \cos \theta}{[(x - R_2 \cos \theta)^2 + (y - R_2 \sin \theta \cos \beta)^2 + (z - R_2 \sin \theta \sin \beta - d)^2]^{3/2}} d\theta, \\ T_{z2} &= \frac{R_2}{4\pi} \int_0^{2\pi} \frac{R_2 \cos \beta - x \cos \beta \cos \theta - y \sin \theta}{[(x - R_2 \cos \theta)^2 + (y - R_2 \sin \theta \cos \beta)^2 + (z - R_2 \sin \theta \sin \beta - d)^2]^{3/2}} d\theta. \end{aligned} \right. \quad (12)$$

where β is the rotation angle of the Rx.

3. QUANTITATIVE ANALYSIS OF APD OF AN MCR WPT SYSTEM

As the expressions of the EDCs of the three MCR WPT systems are consistent, below only the quantitative analysis of the APDs of the most common aligned system (see Figure 4) in practical applications is conducted. Due to the symmetry, the Cartesian coordinate system is converted to a cylindrical coordinate system. The expressions of the EMF and electromagnetic energy density are respectively changed to

$$\mathbf{E} = - \left(P_{\phi 1} \frac{\partial i_1}{\partial t} + P_{\phi 2} \frac{\partial i_2}{\partial t} \right) \cdot \mathbf{e}_\phi, \quad \mathbf{H} = (T_{\rho 1} i_1 + T_{\rho 2} i_2) \cdot \mathbf{e}_\rho + (T_{z 1} i_1 + T_{z 2} i_2) \cdot \mathbf{e}_z. \quad (13)$$

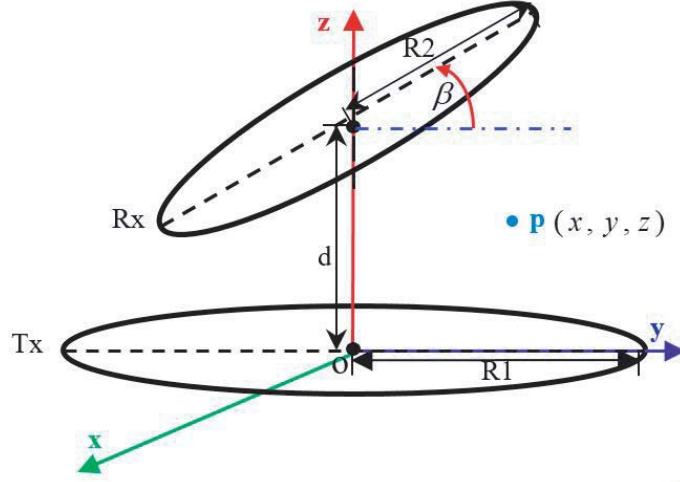


Figure 3. MCR WPT system with a Rx rotation angle of β .

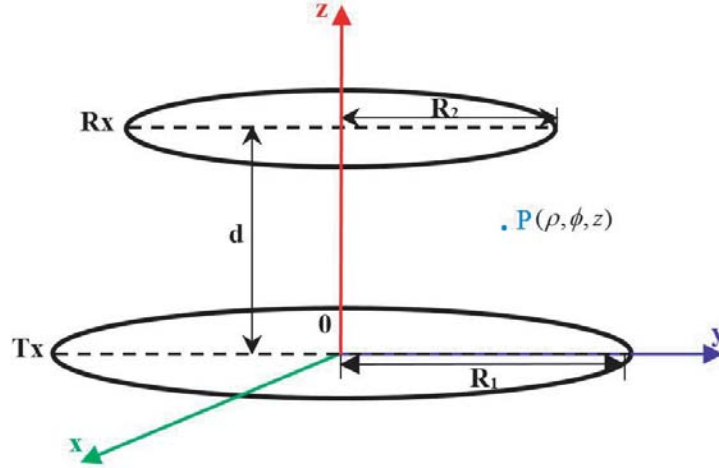


Figure 4. Point p around an aligned MCR WPT system.

where

$$\begin{cases} P_{\phi i} = \frac{\mu_0 R_i}{4\pi} \int_0^{2\pi} \frac{\cos \theta}{\sqrt{R_i^2 + \rho^2 + [(i-1) \cdot d - z]^2 - 2R_i \rho \cos \theta}} d\theta, \\ T_{\rho i} = \frac{R_i}{4\pi} \int_0^{2\pi} \frac{[(i-1) \cdot d - z] \cos \theta}{[R_i^2 + \rho^2 + [(i-1) \cdot d - z]^2 - 2R_i \rho \cos \theta]^{3/2}} d\theta, \\ T_{z i} = \frac{R_i}{4\pi} \int_0^{2\pi} \frac{R_i^2 + [(i-1) \cdot d - z]^2 - R_i \rho \cos \theta}{\rho [R_i^2 + \rho^2 + [(i-1) \cdot d - z]^2 - 2R_i \rho \cos \theta]^{3/2}} \cdot \cos \theta d\theta, \end{cases} \quad (i = 1, 2).$$

And the APD is

$$\mathbf{S}_{av} = \omega I_1 I_2 \sin \alpha \cdot [(P_{\phi 1} T_{z 2} - P_{\phi 2} T_{z 1}) \cdot \mathbf{e}_\rho + (P_{\phi 2} T_{\rho 1} - P_{\phi 1} T_{\rho 2}) \cdot \mathbf{e}_z] \quad (14)$$

For a coupler with $R_1 = R_2 = R$, take a side surface S_3 (like surface 1, 2, 3 in Figure 5(a)) of a cylinder symmetric about the central plane 4 and with the z -axis as its central axis and radius R_s ($R_s > R$). Suppose that there is a pair of points p and p' symmetric about the median plane 4 on the side surface, there is always

$$(P_{\phi 1} T_{z 2})|_p - (P_{\phi 2} T_{z 1})|_p + (P_{\phi 1} T_{z 2})|_{p'} - (P_{\phi 2} T_{z 1})|_{p'} = 0 \quad (15)$$

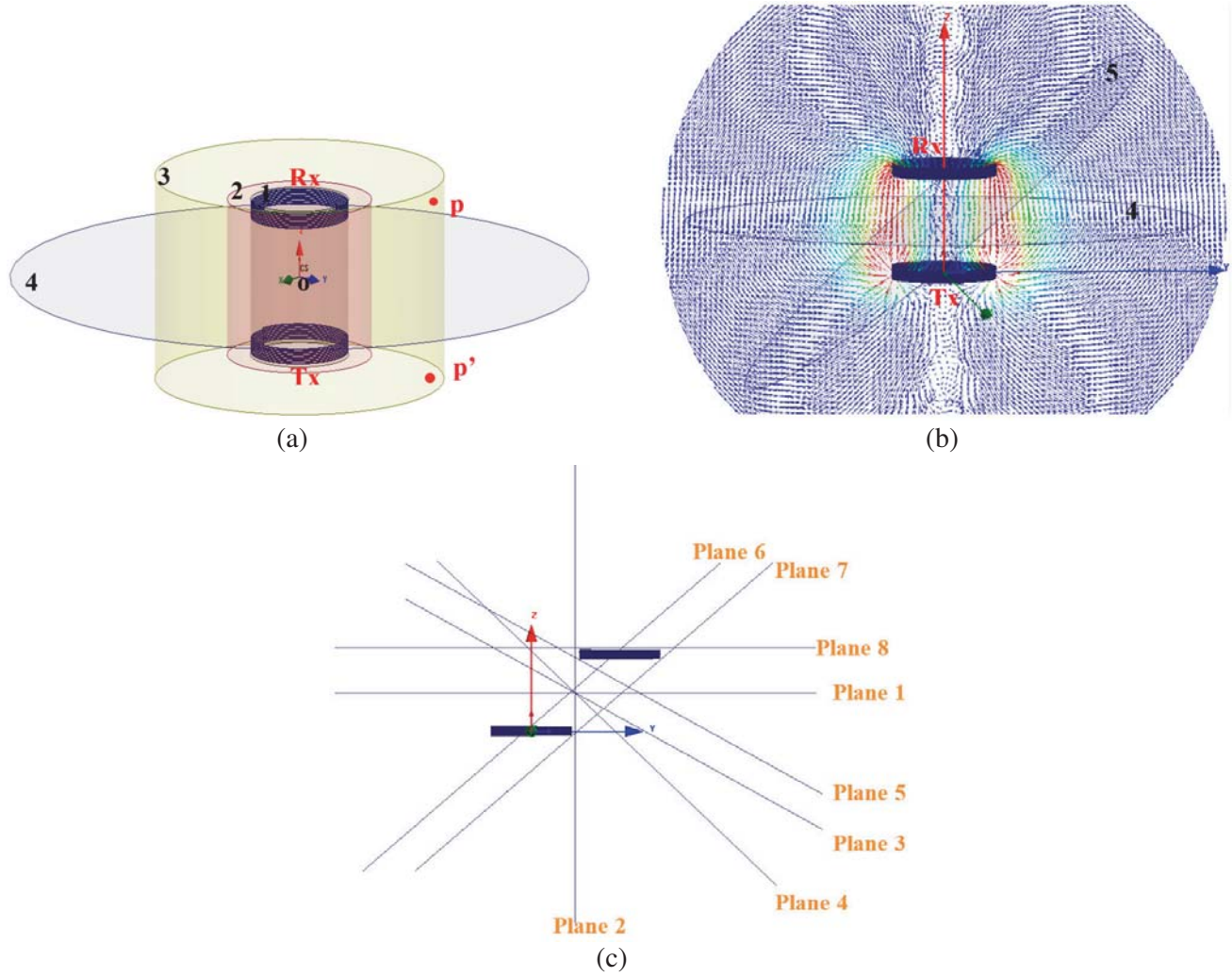


Figure 5. Surfaces around MCR WPT systems. (a) Four surfaces 1, 2, 3 and 4 around an aligned system and points p and p' symmetric about central plane 4; (b) Planes 4 and 5 which intersect the transmission path but do not intersect the coupler and have an area with the radius greater than 5 times the radius of coupler. (c) Planes 1, 2, 3, 4 and 5 that satisfies the similar conditions of Plane 4 (or 5) in (b), Plane 6 which intersects the coupler, and Planes 7 and 8 which do not intersect the transmission path around a MCR WPT system with a lateral misalignment.

Then, we can get

$$\int_{S_3} \mathbf{S}_{av} \cdot d\mathbf{S} = 0 \tag{16}$$

which indicates that the total active power of the WPT system radiating outward through the surface S_3 is zero.

The active power through the central plane 4 with infinite radius is

$$\begin{aligned} P_t &= \int_{S_4} \mathbf{S}_{av} \cdot d\mathbf{S} = \int_0^{+\infty} \mathbf{S}_{av} \cdot \mathbf{n} dS \\ &= \omega I_1 I_2 \sin \alpha \cdot \int_0^{+\infty} \left[(P_{\phi 2} T_{\rho 1}) \Big|_{z=\frac{d}{2}} - (P_{\phi 1} T_{\rho 2}) \Big|_{z=\frac{d}{2}} \right] \cdot 2\pi\rho \cdot d\rho \end{aligned} \tag{17}$$

By numerical integration in MATLAB, the correctness of the following formula is verified under different

sizes and transmission distances of couplers.

$$\int_0^{+\infty} \left[(P_{\phi_2 T_{\rho 1}}) \Big|_{z=\frac{d}{2}} - (P_{\phi_1 T_{\rho 2}}) \Big|_{z=\frac{d}{2}} \right] \cdot 2\pi\rho \cdot d\rho = M \quad (18)$$

where M represents the mutual inductance between the Tx and Rx. During numerical calculation, the upper limit of the integral of ρ is specifically set to 5 times of the radius of coupler. The results satisfy the error requirement. Then Eq. (17) is simplified as

$$P_t = \omega M I_1 I_2 \sin \alpha \quad (19)$$

which is consistent with the expression obtained by reflected load theory in [23]. Actually, the active power passing through any infinity plane (like Plane 5 in Figure 5(b)) which intersects the transmission path but does not intersect the coupler is equal to the transmitted active power. It is also applicable to other non-aligned systems. It is found by simulation that the integral of the active power density passing through the 1 (or 2, or 3, or 4, or 5) in Figure 5(c) is equal to the transmitted active power, whereas the integral of the active power density passing through plane 6 (or 7, or 8) is not equal to the transmitted active power.

Next four basic reactive power compensations are considered. As the phase differences depend only on the secondary compensation schemes, the four basic compensations are divided into two categories: (1) series compensation is adopted on the secondary side including SS and PS schemes; (2) parallel compensation is adopted on the secondary side including SP and PP schemes. Figure 6 presents four systems with four reactive power compensations in which u_{in} is the input voltage; L_1 (L_2), C_1 (C_2) and R_P (R_S) are the inductance, tuning capacitance, and equivalent ac resistance of the Tx (Rx), respectively; and R_L is the load. For the MCR WPT system with series compensation in the secondary circuit (i.e., SS or PS in the Figures 6(a) and (b)), when the system is working stably and resonated, i.e., $\omega L_i = \frac{1}{\omega C_i}$ ($i = 1, 2$), the following relationship is obtained by frequency-domain method,

$$\dot{I}_2 = -j \frac{\omega M}{R_L} \dot{I}_1 \quad (20)$$

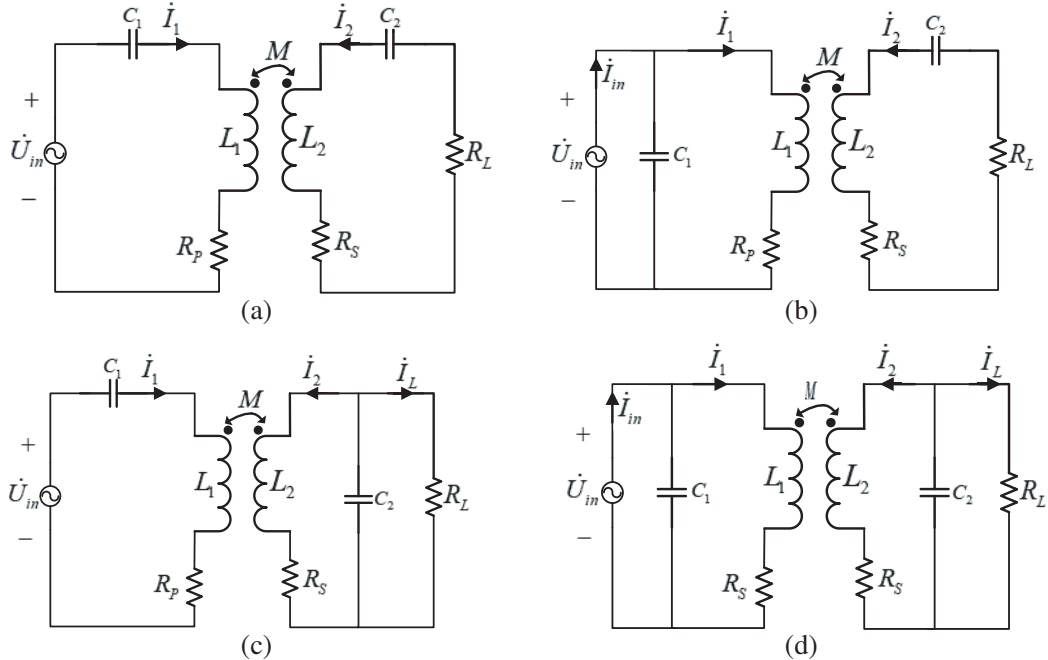


Figure 6. Four basic compensation schemes for WPT system. (a) Primary series-second series (SS). (b) Primary parallel-second series (PS). (c) Primary series-second parallel (SP). (d) Primary parallel-second parallel (PP).

where \dot{I}_1 (\dot{I}_2) is the vector of i_1 (i_2). So there is always $\alpha = \pi/2$, thus the APD at each point is the largest. Meanwhile, the interactive RPD between the Tx and Rx is zero.

For the MCR WPT system with parallel compensation in the secondary circuit (i.e., SP or PP in Figures 6(c) and (d)), when the system is working stably, the following relationship is obtained,

$$\dot{I}_2 = -j \frac{\omega M}{Z_2} \cdot I_1 \quad (21)$$

where $Z_2 = R_S + j\omega L_2 + \frac{R_L}{1+j\omega C_2 R_L}$. In order to improve the PTE of the system, the quality factor of the coil is generally large, and hence there is $R_S \ll R_L$ and $R_S \ll \omega L_2$. The influence of R_S on the output power is small, so it can be ignored during analysis [24]. On the condition of the resonance, i.e., $\omega L_i = \frac{1}{\omega C_i}$ ($i = 1, 2$),

$$\dot{I}_2 = -j \frac{M}{L_2} \left(\frac{R_L}{\omega L_2} - j \right) \cdot I_1 \quad (22)$$

For light loads, i.e., $R_L \ll \omega L_2$, $\dot{I}_2 \approx -\frac{M}{L_2} \cdot I_1$, thus $\alpha = \pi$. For heavy loads, i.e., $R_L \gg \omega L_2$, $\dot{I}_2 \approx -j \frac{MR_L}{\omega L_2^2} \cdot \dot{I}_1$, thus $\alpha = \pi/2$. So it is recommended to use heavy load in the MCR WPT system with parallel compensation on the secondary side to make α tend to be $\pi/2$.

Then the PTE is analyzed to verify that heavy load contributes to power transfer. The PTE of the MCR WPT system with parallel on the second side is

$$\eta = \frac{I_L^2 R_L}{I_1^2 R_P + I_2^2 R_S + I_L^2 R_L} = \frac{\omega L_2 / R_S}{\frac{R_L}{\omega L_2} + \frac{1 + \frac{L_2^2 R_P}{M^2 R_S}}{\frac{R_L}{\omega L_2}} + \omega L_2 / R_S} \quad (23)$$

Then $\frac{R_L}{\omega L_2}$ corresponding to the extreme value point of the η is solved as

$$\frac{R_L}{\omega L_2} = \sqrt{\frac{M^2 + L_2^2 R_P / R_S}{M^2}} \quad (24)$$

Considering the general MCR WPT systems with the Tx and Rx of the same circuit parameters, i.e., $R_P = R_S$, Eq. (24) is simplified to

$$\frac{R_L}{\omega L_2} = \sqrt{1 + \frac{L_2^2}{M^2}} \quad (25)$$

Generally, $L_2 \gg M$, Eq. (24) is further simplified to

$$\frac{R_L}{\omega L_2} = \frac{L_2}{M} \quad (26)$$

As $L_2 \gg M$, the condition of $\frac{R_L}{\omega L_2} < \frac{L_2}{M}$ is satisfied for a general system. Accordingly, the PTE will increase with the increase of R_L in the MCR WPT system with SP (or PP) compensation.

Finally, the directionality of the APD is to be explored, and the APD is utilized to explain the coupling impedance. Coupling impedance as a lumped parameter of the system can be expressed as

$$Z_{Coupling} = \frac{\dot{U}_{2in}}{\dot{I}_1} = j\omega M \quad (27)$$

where \dot{U}_{2in} is the input voltage on the Rx. When the Rx is horizontally offset or rotated by a certain angle, and the coupling impedance decreases, the transmission path of the APD is more indirect from the perspective of electromagnetic fields (see Figure 7). In Figure 7, the currents in the Tx (or Rx) for the three MCR WPT systems are set the same which can be achieved by adjusting circuit parameters such as input voltage or load. The APD of the systems with a lateral and angular misalignment is normalized to the APD of the alignment system for comparison at equal transmission active power.

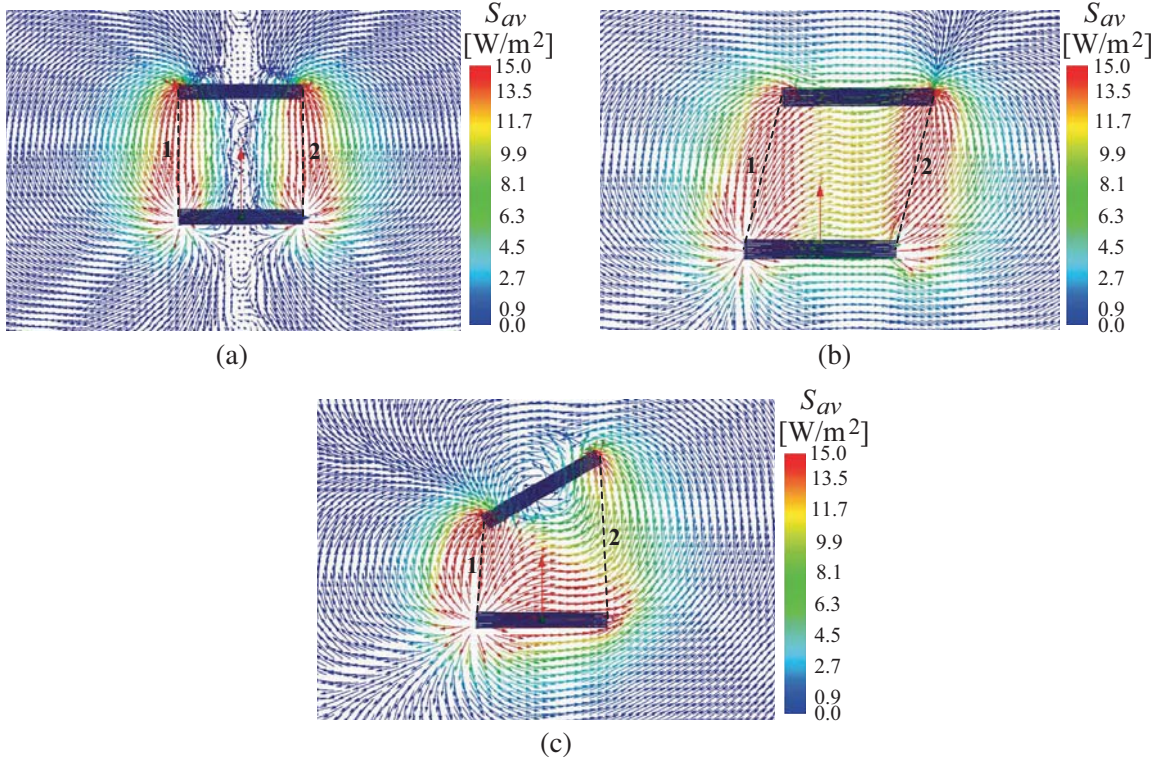


Figure 7. APD distribution of three MCR WPT systems with identical currents in Tx (or Rx). (a) Aligned system with the mutual inductance of $0.947 \mu\text{H}$. (b) System with an Rx horizontal offset distance of $l = R/2$ and the mutual inductance of $0.853 \mu\text{H}$. (c) System with an Rx rotation angle of $\beta = \pi/6$ and the mutual inductance of $0.863 \mu\text{H}$.

It is found that the energy flow of the system is clearly directional, that is, from Tx to Rx, but the transmission path or direction of the APD is very irregular, depending on the relative position of the Tx and Rx. The APD of the alignment system is relatively straightforward, and the path is short, whereas the paths of other systems are long. In addition, Figure 7 reveals that the APDs are mainly distributed around the dotted lines 1 and 2 in the transmission path, which may result in high EMF values outside the main energy transfer area and thus may threaten the electromagnetic safety of people around the MCR WPT system.

4. SIMULATION AND EXPERIMENTAL VERIFICATIONS

To illustrate the correctness of the theoretical calculation, the theoretical calculation values of the energy density (including APD and RPD) of an MAC WPT system with the offset distance of $l = R/2$ and $\alpha = \pi/2$ are compared with the simulated values. At this time, the total APD and RPD around the system are respectively changed to

$$\begin{aligned} \mathbf{S}_{av} = & \omega I_1 I_2 \cdot [(P_{y1} T_{z2} - P_{y2} T_{z1}) \cdot \mathbf{e}_x + (P_{x2} T_{z1} - P_{x1} T_{z2}) \cdot \mathbf{e}_y \\ & + (P_{x1} T_{y2} - P_{x2} T_{y1} + P_{y2} T_{x1} - P_{y1} T_{x2}) \cdot \mathbf{e}_z] \end{aligned} \quad (28)$$

$$\begin{aligned} \mathbf{S}_{im} = & \omega [(-I_1^2 P_{y1} T_{z1} + I_2^2 P_{y2} T_{z2}) \cdot \mathbf{e}_x + (I_1^2 P_{x1} T_{z1} - I_2^2 P_{x2} T_{z2}) \cdot \mathbf{e}_y \\ & + (-I_1^2 P_{x1} T_{y1} + I_2^2 P_{x2} T_{y2} + I_1^2 P_{y1} T_{x1} - I_2^2 P_{y2} T_{x2}) \cdot \mathbf{e}_z] \end{aligned} \quad (29)$$

The simulated values are obtained by ANSYS MAXWELL. As frequency-domain method is adopted in the solution type of eddy current in the software, first it is necessary to derive the frequency-domain expressions of the APD and RPD.

Convert Eq. (4) from the time domain to frequency domain, and there is

$$\begin{aligned}\dot{\mathbf{E}} &= \dot{\mathbf{E}}_1 + \dot{\mathbf{E}}_2 = -j\omega \cdot \left[\left(P_{x1}\dot{I}_1 + P_{x2}\dot{I}_2 \right) \cdot \mathbf{e}_x + \left(P_{y1}\dot{I}_1 + P_{y2}\dot{I}_2 \right) \cdot \mathbf{e}_y \right], \\ \dot{\mathbf{H}} &= \dot{\mathbf{H}}_1 + \dot{\mathbf{H}}_2 = \left(T_{x1}\dot{I}_1 + T_{x2}\dot{I}_2 \right) \cdot \mathbf{e}_x + \left(T_{y1}\dot{I}_1 + T_{y2}\dot{I}_2 \right) \cdot \mathbf{e}_y + \left(T_{z1}\dot{I}_1 + T_{z2}\dot{I}_2 \right) \cdot \mathbf{e}_z.\end{aligned}\quad (30)$$

Then it can be obtained from $\dot{\mathbf{S}} = \dot{\mathbf{E}} \times \dot{\mathbf{H}}^*$ that

$$\begin{aligned}\dot{\mathbf{S}} &= \dot{\mathbf{S}}_{p11} + \dot{\mathbf{S}}_{p22} + \dot{\mathbf{S}}_{p12} + \dot{\mathbf{S}}_{p21} \\ &= -j\omega I_1^2 \cdot [P_{y1}T_{z1} \cdot \mathbf{e}_x - P_{x1}T_{z1} \cdot \mathbf{e}_y + (P_{x1}T_{y1} - P_{y1}T_{x1}) \cdot \mathbf{e}_z] \\ &\quad -j\omega I_2^2 \cdot [P_{y2}T_{z2} \cdot \mathbf{e}_x - P_{x2}T_{z2} \cdot \mathbf{e}_y + (P_{x2}T_{y2} - P_{y2}T_{x2}) \cdot \mathbf{e}_z] \\ &\quad -j\omega I_1 I_2 e^{j\alpha} \cdot [P_{y1}T_{z2} \cdot \mathbf{e}_x - P_{x1}T_{z2} \cdot \mathbf{e}_y + (P_{x1}T_{y2} - P_{y1}T_{x2}) \cdot \mathbf{e}_z] \\ &\quad -j\omega I_1 I_2 e^{-j\alpha} \cdot [P_{y2}T_{z1} \cdot \mathbf{e}_x - P_{x2}T_{z1} \cdot \mathbf{e}_y + (P_{x2}T_{y1} - P_{y2}T_{x1}) \cdot \mathbf{e}_z]\end{aligned}\quad (31)$$

when $\alpha = \pi/2$,

$$\begin{aligned}\text{Re}(\dot{\mathbf{S}}) &= \omega I_1 I_2 \cdot [(P_{y1}T_{z2} - P_{y2}T_{z1}) \cdot \mathbf{e}_x \\ &\quad + (P_{x2}T_{z1} - P_{x1}T_{z2}) \cdot \mathbf{e}_y + (P_{x1}T_{y2} - P_{x2}T_{y1} + P_{y2}T_{x1} - P_{y1}T_{x2}) \cdot \mathbf{e}_z]\end{aligned}\quad (32)$$

which is consistent with Eq. (28).

$$\begin{aligned}\text{Im}(\dot{\mathbf{S}}) &= \omega [(-I_1^2 P_{y1}T_{z1} - I_2^2 P_{y2}T_{z2}) \cdot \mathbf{e}_x + (I_1^2 P_{x1}T_{z1} + I_2^2 P_{x2}T_{z2}) \cdot \mathbf{e}_y \\ &\quad + (-I_1^2 P_{x1}T_{y1} - I_2^2 P_{x2}T_{y2} + I_1^2 P_{y1}T_{x1} + I_2^2 P_{y2}T_{x2}) \cdot \mathbf{e}_z]\end{aligned}\quad (33)$$

The RPD formulas of the time domain and frequency domain are not consistent, but the RPDs generated separately by Tx (or Rx) and calculated by the two methods are the same. Actually, when $\alpha = 0$, the total RPD around the MCR WPT system obtained by the time-domain method is changed to

$$\begin{aligned}\mathbf{S}_{im}|_{\alpha=0} &= \omega [(-I_1^2 P_{y1}T_{z1} - I_2^2 P_{y2}T_{z2}) \cdot \mathbf{e}_x + (I_1^2 P_{x1}T_{z1} + I_2^2 P_{x2}T_{z2}) \cdot \mathbf{e}_y \\ &\quad + (-I_1^2 P_{x1}T_{y1} - I_2^2 P_{x2}T_{y2} + I_1^2 P_{y1}T_{x1} + I_2^2 P_{y2}T_{x2}) \cdot \mathbf{e}_z]\end{aligned}\quad (34)$$

which is consistent with Eq. (33). Therefore, the results obtained by the time-domain method are reasonable as it can reflect the change in the total RPD for different phase differences, and there is always $S_{im} \leq \text{Im}(\dot{\mathbf{S}})$. The equation is true only when the phases of the currents are equal. The comparison of theoretical calculation and simulation values of the APD and RPD are presented in Figure 8.

During the calculation and simulation, the turns of the coils are 8, but the geometric differences of every turn of the coils are ignored for convenience during the theoretical calculation. The parameters of the MCR WPT system can be referred to Table 1.

Table 1. Parameters of an MCR WPT System with a lateral misalignment.

Geometric and material parameters	Physical meanings	Values
R	Radius of the Tx (Rx)	100 mm
d	Transmission distance	200 mm
N_s	Number of turns of each coil	8
l	Offset distance	50 mm
α	Lagging phase of the current in Rx behind the current in Tx	$\pi/2$
μ_0	Magnetic permeability of air	$4\pi \times 10^{-7}$
f_0	Resonance frequency	270 kHz

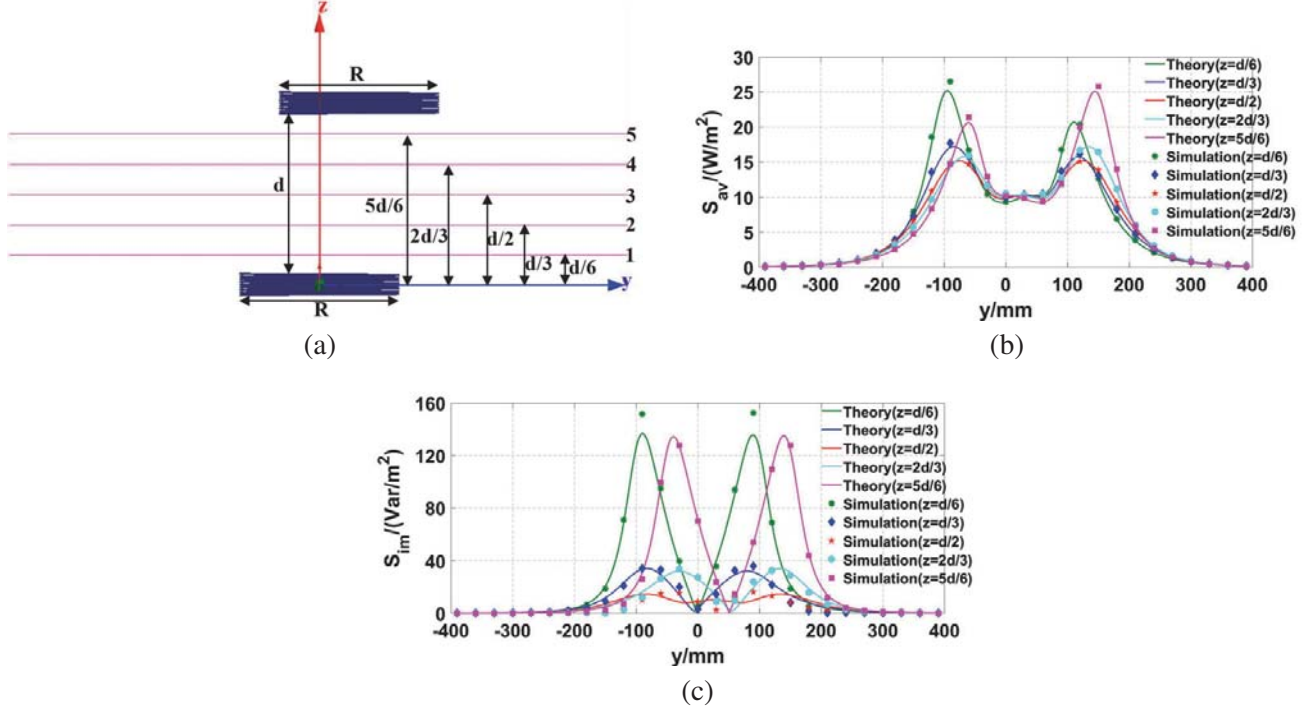


Figure 8. Comparison of theoretical calculation and simulation values of APD and RPD. (a) System with an Rx horizontal offset distance of $l = R/2$ and five lines on which the APD and RPD values are measured. (b) APD. (c) RPD.

Figure 8(b) shows that the theoretical values of the APD are consistent with the simulated values, except at points of $z = d/6$, $y = \pm 90$ mm and $z = 5d/6$, $y = -60$ or 150 mm, which is because the geometric differences of every turn of the coils are ignored during the theoretical calculation, and the points are close to the coils. This illustrates the correctness of theoretical calculations. Furthermore, from $z = d/6$ to $z = 5d/6$, the y value corresponding to the right maximum APD points on the five lines gradually changes from 100 mm (i.e., R) to 150 mm (i.e., $R + l$), which can be obviously observed in the APD distribution in the transmission path in Figures 9(a) and (b).

Since the RPD approximately satisfies $\frac{1}{r^3}$ attenuation with r , the differences of the RPD between the theoretical calculation and simulation are small in the vicinity of the coils like Lines 1 and 5 (except at points of $z = d/6$, $y = \pm 90$ mm owing to the reasons mentioned above), Whereas the differences in Line 3 are large, which is mainly due to the difference in expressions obtained by time-domain and frequency-domain method. It can also be found that the maximum RPD values on the five lines are all close to the Litz wires of the coils, which can be more clearly observed in Figures 9(c) and (d).

In addition, Figure 9 reveals that the APD is concentrated in the transmission path of the MCR WPT system, and the RPD is gradually attenuated outwardly around the Litz wires of the coils. Consistency between the APD and RPD distributions obtained by theoretical calculation and simulation further illustrates the correctness of the theoretical calculation. Meanwhile, the direction of the energy flow (APD and RPD) is presented in the simulation results.

Next the phase differences between the currents in the Tx and Rx and PTEs of an aligned MCR WPT system with SP compensation are explored with the change of the load by experiment, and the influences of different transmission distances are also considered. In the experiment, the switching frequency for the inverter is set to 270 kHz; the utilized switching device is IRF640N; and the input voltage of the DC power supply is fixed at 10 V. The experimental process and currents waveforms are shown in Figure 10. The specific parameters of the system are presented in Table 2. The PTEs of the system are calculated by the following formula by measuring the currents in the Tx and Rx and through

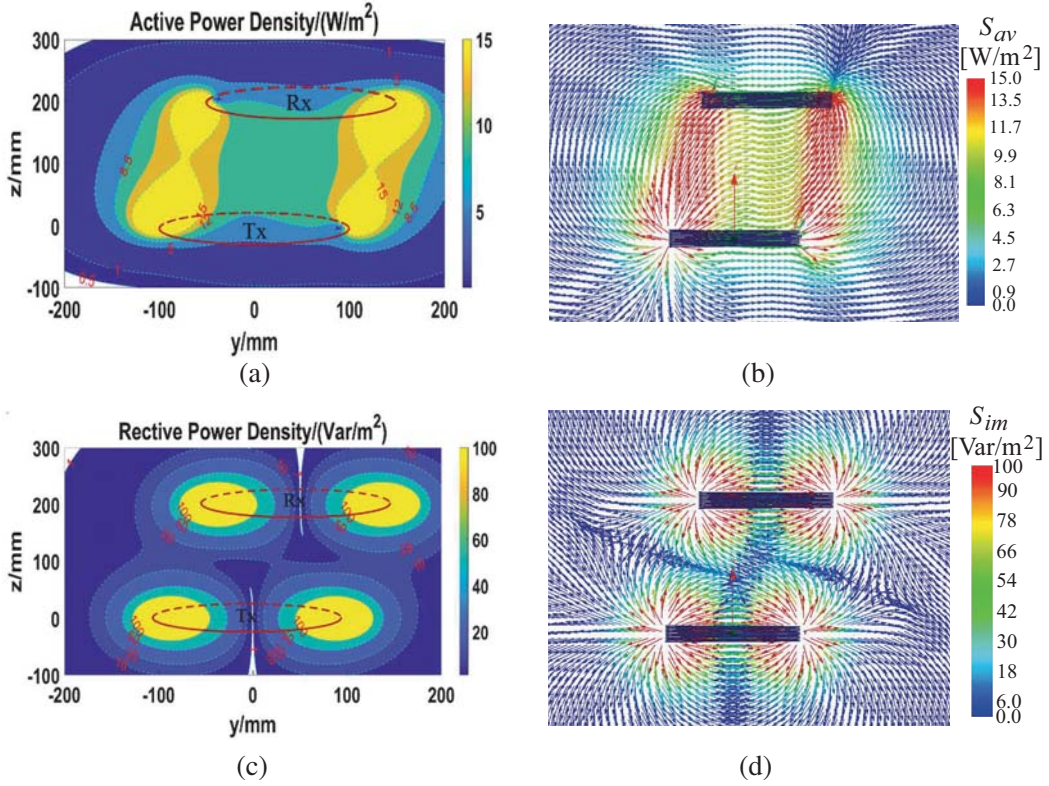


Figure 9. APD and RPD distribution obtained by theoretical calculation and simulation. APD: (a) theoretical calculation (The white area indicates that the values are smaller than 0.5); (b) simulation; RPD: (c) theoretical calculation (The white area indicates that the values are smaller than 1); (d) simulation.

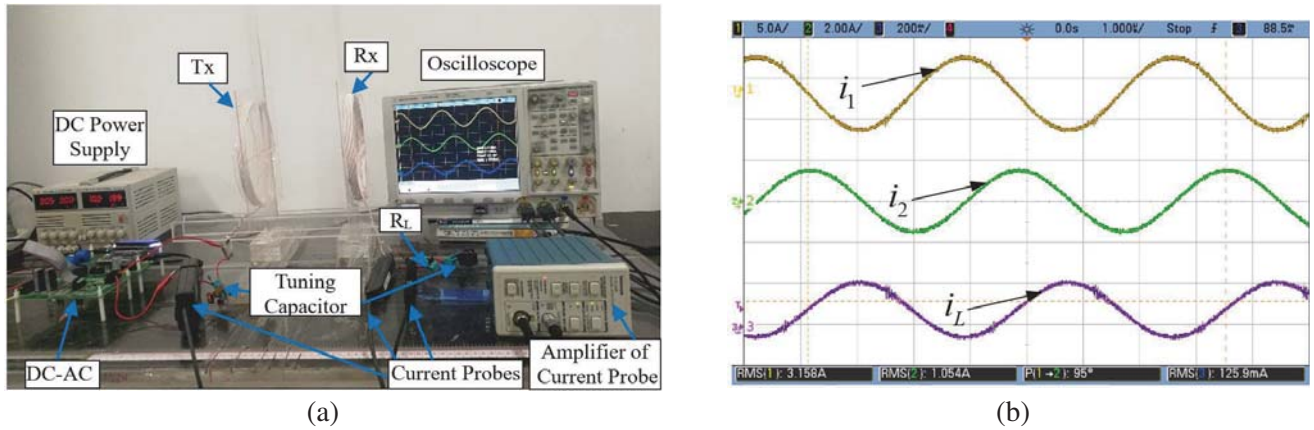


Figure 10. Experimental measurement process. (a) Experiment setup of the MCR WPT system with SP compensation. (b) Currents in the Tx, Rx and through the load when the transmission distance is $2R$ and the impedance of the load approximately equals $10\omega L$.

the load for different loads and transmission distances.

$$\eta = \frac{I_L^2 R_L}{I_1^2 R_P + I_2^2 R_S + I_L^2 R_L} \tag{35}$$

Meanwhile, the lagging phases of the currents in the Rx behind the currents in Tx are recorded.

The transmission distances are taken as R , $2R$, $3R$, and $4R$, and the range of load impedance is $0.05\omega L_2 \sim 21.5\omega L_2$. The phase differences and PTEs of the system which vary with the ratio of the load to ωL_2 for different transmission distances are respectively presented in Figures 11 and 12.

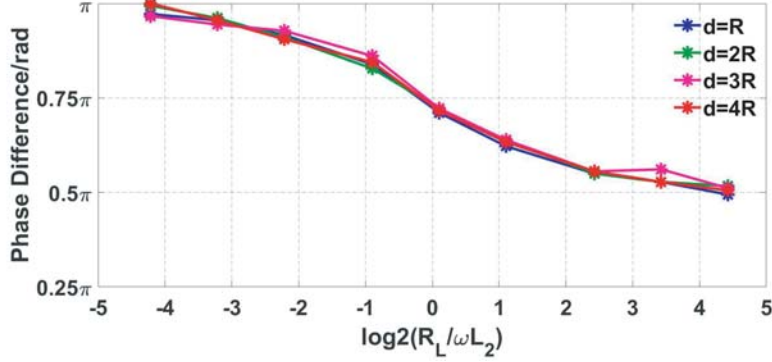


Figure 11. Changes in phase differences with $R_L/\omega L_2$ for different transmission distances.

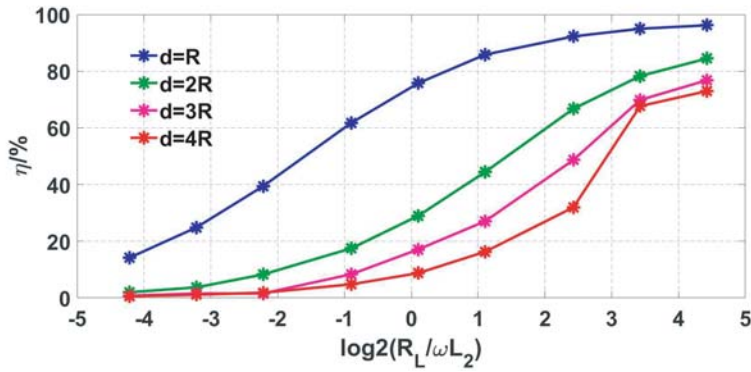


Figure 12. PTE changes with $R_L/\omega L_2$ for different transmission distances.

Table 2. Parameters of an aligned MCR WPT system with a SP compensation.

Geometric and circuit parameters	Physical meanings	Values
R	Radius of the Tx (Rx)	100 mm
d	Transmission distance	$R/2R/3R/4R$
N_s	Number of turns of each coil	8
$L_1(L_2)$	Inductance of the Tx (Rx)	27.41 μ H
$C_1(C_2)$	Tuning capacitance of the Tx (Rx)	12.68 nF
$R_P(R_S)$	Equivalent ac resistance of Tx (Rx)	0.199 Ω
U_s	Voltage RMS value of DC power Supply	10 V
R_L	Load	$0.05\omega L_2 \sim 21.5\omega L_2$
α	Lagging phase of the current in Rx behind the current in Tx	To be determined
f_0	Resonance frequency	270 kHz

Figure 11 presents that for the MCR WPT system with SP compensation, the phase difference tends to be $\pi/2$ as the load increases for different transmission distances. Figure 12 verifies that as the load increases, i.e., the phase difference approaches $\pi/2$, the PTE of the system increases for different transmission distances, and for the same load, the closer the distance is, the greater the PTE is.

5. CONCLUSION

The EDCs of three systems including an aligned system and systems with an angular and lateral misalignment are explored based on Poynting vector theory by the time-domain method, and unified expressions of APD and RPD are provided. As a verification, the expressions obtained by the frequency-domain method are also derived. It is found that the formulas of the APD obtained by the two methods are consistent, and the expression of the RPD generated by separately the Tx (or Rx) is also consistent. Furthermore, the APD is mainly distributed in the transmission path, and the RPD is composed of three parts, two of which are respectively generated by Tx and Rx, and the third part is the interactive RPD, depending on whether the phase difference (α) between the currents in the Tx and Rx is $\pi/2$. Then, quantitative analysis of the APD shows that the total active power radiated outward the cylinder surface coaxial with the system is zero. The active power through an arbitrary infinite plane which intersects the transmission path but does not intersect the coupler is equal to the transferred active power of the system, which is consistent with the results obtained by the circuit theory. Meanwhile, it is found that APD is proportional to $\sin\alpha$, and when the phase difference is $\pi/2$, the value is the largest. So a phase difference of $\pi/2$ between the currents in the Tx and Rx contributes to energy transfer. Furthermore, the APD is utilized to explain the coupling impedance in circuit theory. The APD distribution has a clear directionality, that is, from Tx to Rx. However, the transmission path of APD is very irregular, depending on the position of the relative position of the Tx and Rx, but it is independent of the working condition, that is, independent of the amplitudes and phase differences of the currents. It is found that the APD of the aligned system with large coupling impedance is relatively straight, and the transmission path is short, whereas the other APD paths of the non-aligned systems with small coupling impedance are long. The simulation results verify the theoretical calculation of the EDCs.

Then combined with four basic reactive power compensations, the current phase differences are explored. For the system with series compensation on the secondary side (SS or PS), when the system is harmonic, the phase difference is always $\pi/2$, whereas for the system with parallel compensation on the secondary side (SP or PP), the phase difference tends to be $\pi/2$ at heavy loads and tends to be π at light loads. Therefore, it is recommended to use heavy load for the MCR WPT system with parallel compensation on the secondary side. Circuit analysis and an experiment are conducted, which verify that for different transmission distances, as the load increases the phase difference tends to be $\pi/2$, and the PTEs increases accordingly.

Future work could be done to design the coils of the MCR WPT system to concentrate the energy inside the main transmission area to reduce high EMF values outside the main energy transfer area as much as possible, and measures such as adding small coils inside the spiral coils can be employed.

ACKNOWLEDGMENT

This work was supported financially by the National Natural Science Foundation of China (Grant No. 51477014).

REFERENCES

1. Li, S. and C. C. Mi, "Wireless power transfer for electric vehicle applications," *IEEE J. Emerg. Sel. Topics Power Electron.*, Vol. 3, No. 1, 4–17, 2015.
2. Sergeant, P. and A. V. D. Bossche, "Inductive coupler for contactless power transmission," *IET Elect. Power Appl.*, Vol. 2, No. 1, 1–7, 2008.
3. Omer Onar, C., et al., "Oak ridge national laboratory wireless charging of electric vehicles — CRADA report," *Tech. Rep.*, Oak Ridge National Lab., Oak Ridge, TN, USA, TM-2016-296, 2016.

4. Kim, J. W., H.-C. Son, D.-H. Kim, and Y.-J. Park, "Optimal design of a wireless power transfer system with multiple self-resonators for an LED TV," *IEEE Transactions on Consumer Electronics*, Vol. 58, No. 3, 775–780, 2012.
5. Choi, B., J. Nho, H. Cha, T. Ahn, and S. Choi, "Design and implementation of low-profile contactless battery charger using planar printed circuit board windings as energy transfer device," *IEEE Trans. Ind. Electron.*, Vol. 51, No. 1, 140–147, 2004.
6. Li, Q. and Y. C. Liang, "An inductive power transfer system with a high-Q resonant tank for mobile device charging," *IEEE Trans. Power Electron.*, Vol. 30, No. 11, 6203–6212, 2015.
7. Basar, M. R., M. Y. Ahmad, J. Cho, and F. Ibrahim, "Stable and high efficiency wireless power transfer system for robotic capsule using a modified Helmholtz coil," *IEEE Trans. Ind. Electron.*, Vol. 64, No. 2, 1113–1122, 2017.
8. Park, S. I., "Enhancement of wireless power transmission into biological tissues using a high surface impedance ground plane," *Progress In Electromagnetics Research*, Vol. 135, 123–136, 2013.
9. Simic, M., C. Bil, and V. Vojisavljevic, "Investigation in wireless power transmission for UAV charging," *Procedia Comput. Sci.*, Vol. 60, 1846–1855, 2015.
10. Xu, J., Y. Zeng, and R. Zhang, "UAV-enabled wireless power transfer: Trajectory design and energy optimization," *IEEE Trans. Wireless Commun.*, Vol. 17, No. 8, 5092–5106, 2018.
11. Liu, H. Q., H. C. So, K. W. K. Lui, and F. K. W. Chan, "Sensor selection for target tracking in sensor networks," *Progress In Electromagnetics Research*, Vol. 131, 267–282, 2009.
12. Hong, Y. W. P., T. C. Hsu, and P. Chennakesavula, "Wireless power transfer for distributed estimation in wireless passive sensor networks," *IEEE Trans. Signal Process.*, Vol. 64, No. 20, 5382–5395, 2016.
13. Hui, S. Y. R., "Technical and safety challenges in emerging trends of near-field wireless power transfer industrial guidelines," *IEEE Trans. Electromagn. Compat.*, Vol. 7, No. 1, 78–86, 2018.
14. Lu, F., H. Zhang, H. Hofmann, and C. Mi, "A double-sided LC-compensation circuit for loosely coupled capacitive power transfer," *IEEE Trans. Power Electron.*, Vol. 33, No. 2, 1633–1643, 2018.
15. Pinuela, M., D. C. Yates, S. Lucyszyn, and P. D. Mitcheson, "Maximizing DC-to-load efficiency for inductive power transfer," *IEEE Trans. Power Electron.*, Vol. 28, No. 5, 2437–2447, 2013.
16. Fan, Y., L. Li, S. Yu, C. Zhu, and C.-H. Liang, "Experimental study of efficient wireless power transfer system integrating with highly sub-wavelength metamaterials," *Progress In Electromagnetics Research*, Vol. 141, 769–784, 2013.
17. Deng, Q. J., J. T. Liu, D. Czarkowski, W. S. Hu, and H. Zhou, "An inductive power transfer system supplied by a multiphase parallel inverter," *IEEE Trans. Ind. Electron.*, Vol. 64, No. 9, 7039–7048, 2017.
18. Hao, H., G. A. Covic, and J. T. Boys, "A parallel topology for inductive power transfer power supplies," *IEEE Trans. Power Electron.*, Vol. 29, No. 3, 1140–1151, 2014.
19. Faria, J. B., "Poynting vector flow analysis for contactless energy transfer in magnetic systems," *IEEE Trans. Power Electron.*, Vol. 27, No. 10, 4292–4300, 2012.
20. Liu, Y., A. P. Hu, and U. Madawala, "Determining the power distribution between two coupled coils based on Poynting vector analysis," *IEEE PELS Workshop on Emerging Technologies: Wireless Power Transfer (WoW)*, Chongqing, China, May 20–22, 2017.
21. Guo, Y. S., et al., "Poynting vector analysis for wireless power transfer between magnetically coupled coils with different loads," *Sci. Rep.*, Vol. 7, No. 741, 1–6, 2017.
22. Jin, J.-M., *Theory and Computation of Electromagnetic Fields*, Wiley, Hoboken, 2010.
23. Kiani, M., U. Jow, and M. Ghovanloo, "Design and optimization of a 3-coil inductive link for efficient wireless power transmission," *IEEE Trans. Biomed. Circuits Syst.*, Vol. 5, No. 6, 579–591, 2011.
24. Zhang, B., R.-H. Huang, and X.-J. Shu, *Principle of Wireless Power Transmission*, Science Press, Beijing, 2018.